Supporting information for:

Hybrid and Non-Hybrid Lipids Exert Common Effects on Membrane Raft Size and Morphology

Frederick A. Heberle, Milka Doktorova, Shih Lin Goh, Robert F. Standaert, John Katsaras, and Gerald W. Feigenson

The supporting information consists of six figures, four tables, and one section describing Materials and Methods.

Abbreviations:

BoDIPY-PC	2-(4,4-difluoro-5,7-dimethyl-4-bora-3a,4a-diaza-s-indacene-3-pentanoyl)-1-hexadecanoyl-*sn*-glycero-3-phosphocholine
C12:0-DiI	1,1′-didodecyl-3,3,3′,3′-tetramethylindocarbocyanine perchlorate
Chol	cholesterol
DHE	dehydroergosterol, ergosta-5,7,9(11),22-tetraen-3β-ol
DLPC	1,2-dilauroyl-*sn*-glycero-3-phosphocholine
DOPC	1,2-dioleoyl-*sn*-glycero-3-phosphocholine
DSC	differential scanning calorimetry
DSPC	1,2-distearoyl-*sn*-glycero-3-phosphocholine
DSPC-d70	1,2-distearoyl(d70)-*sn*-glycero-3-phosphocholine
FRET	Förster resonance energy transfer
GUV	giant unilamellar vesicle
Ld	liquid-disordered
Lo	liquid-ordered
LUV	large unilamellar vesicle
MLV	multilamellar vesicle
PLV	paucilamellar vesicle
REE	region of enhanced FRET efficiency
RRE	region of reduced FRET efficiency
RSE	rapid solvent exchange
SAE	sensitized acceptor emission
SANS	small-angle neutron scattering
SLD	neutron scattering length density
TLC	thin-layer chromatography
Vpp	volts peak-to-peak

Table S1 Sample compositions examined in this study.

Composition	Technique	Vesicle prep	χDSPC	χ(DLPC+DOPC)	χChol
A	Fluor. microscopy	GUV	0.5	0.3	0.2
B	Fluor. microscopy	GUV	0.45	0.3	0.25
C	Fluor. microscopy	GUV	0.35	0.4	0.25
D	SANS	LUV	0.39	0.39	0.22
E	SANS	LUV	0.325	0.325	0.35
F	FRET	PLV	0	0.905	0.095
G	FRET	PLV	0.685	0	0.315

Table S2 Microscopy data obtained in this study.

Composition	ρ	Counts (uniform/mod./macro)	Proportions (uniform/mod./macro)	St. Dev. (uniform/mod./macro)
A	0.1	214/1/0	0.955/0.005/0	0.005/0.005/0
A	0.15	293/273/2	0.516/0.481/0.004	0.021/0.021/0.002
A	0.2	58/93/0	0.384/0.616/0	0.040/0.040/0
A	0.25	34/274/12	0.106/0.856/0.038	0.017/0.020/0.011
A	0.3	7/92/107	0.034/0.447/0.519	0.013/0.035/0.035
A	0.35	4/8/111	0.033/0.065/0.902	0.016/0.022/0.027
A	0.355	2/12/147	0.012/0.075/0.913	0.009/0.021/0.022
A	0.4	0/73/39	0/0.652/0.348	0/0.045/0.045
B	0	40/0/0	1/0/0	N/A
B	0.1	59/0/0	1/0/0	N/A
B	0.15	94/34/0	0.734/0.266/0	0.039/0.039/0
B	0.2	26/29/114	0.154/0.172/0.675	0.028/0.029/0.036
B	0.25	24/22/133	0.134/0.123/0.743	0.025/0.025/0.033
B	0.3	10/21/55	0.116/0.244/0.640	0.035/0.046/0.052
B	0.35	21/37/130	0.112/0.197/0.691	0.023/0.029/0.034
B	0.4	69/108/43	0.314/0.491/0.195	0.031/0.034/0.027
C	0.1	35/0/0	1/0/0	N/A
C	0.15	32/0/0	1/0/0	N/A
C	0.2	120/0/0	1/0/0	N/A
C	0.25	172/18/6	0.878/0.092/0.031	0.023/0.021/0.012
C	0.3	59/60/13	0.447/0.455/0.098	0.043/0.043/0.026
C	0.35	44/50/66	0.275/0.313/0.413	0.035/0.037/0.039
C	0.4	5/12/138	0.032/0.077/0.890	0.014/0.021/0.025
C	0.45	0/8/58	0/0.121/0.879	0/0.040/0.040
C	0.5	1/2/90	0.011/0.022/0.968	0.011/0.015/0.018

Table S3 SANS data obtained in this study.

Composition	ρ	Pore diameter (nm)	ULV diameter (nm)	Rel. polydispersity	Domain diameter (nm)
D	0	50	65.2	0.21	18.7
D	0.1	50	60.9	0.23	22.6
D	0.25	50	59.9	0.23	26.5
E	0	50	67.7	0.20	---

Table S4 Comparison of results for hybrid and non-hybrid mixtures.

	Modulated phases in GUVs		Domain diameter (nm) in LUVs				
	DSPC/Chol	ρ	DSPC/Chol	ρ=0	ρ=0.1	ρ=0.2	ρ=0.25
Hybrid[a]	0.375/0.225	0.15-0.40[c]	0.39/0.22	13.6[d]	17[d]	24.8[d]	--
Non-hybrid[b]	0.35/0.25	0.20-0.40	0.39/0.22	18.7	22.6	--	26.5

[a]DSPC/(POPC+DOPC)/Cholesterol. [b]DSPC/(DLPC+DOPC)/Cholesterol. [c]Taken from ref 16. [d]Taken from ref 12.

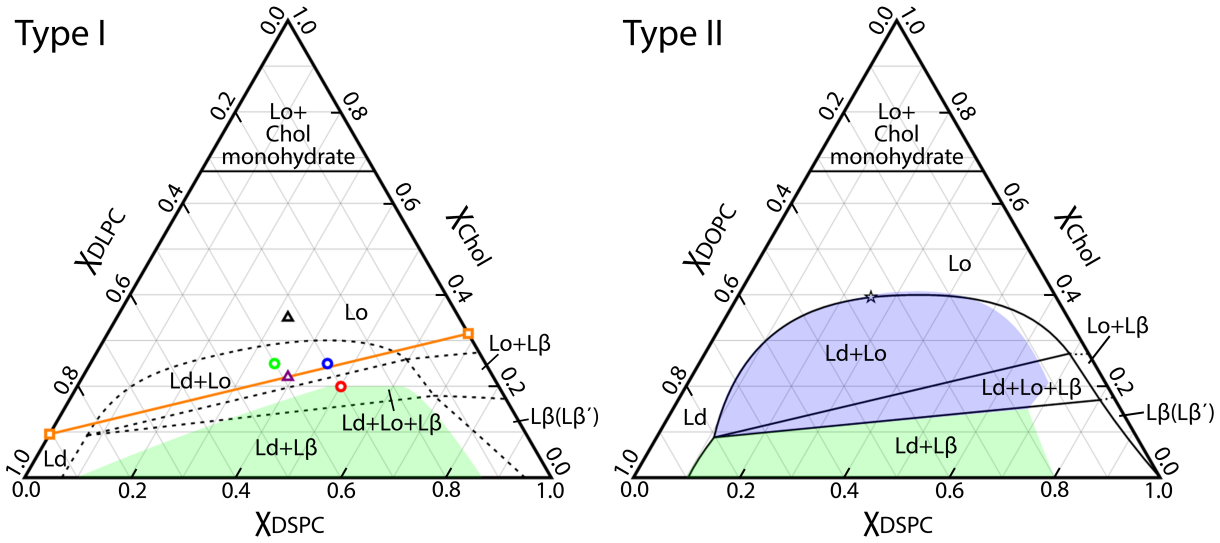

Figure S1 Room temperature phase diagrams for multicomponent lipid bilayer mixtures examined in this study. Phase diagrams for DSPC/DLPC/Chol and DSPC/DOPC/Chol[1] are respectively classified as Type I or Type II[2] to indicate the number of microscopic phase coexistence regions (shaded green and blue areas), where micron-sized domains are visible with fluorescence microscopy.[1,3] Compositions examined in this study include: A, B and C (red, blue and green circles, respectively), with fluorescence microscopy; D and E (purple and black triangles, respectively), with SANS; and a sample trajectory (orange line) prepared from endpoints F and G (orange squares), with FRET. All sample compositions are listed in Table S1. Dashed phase boundaries for DSPC/DLPC/Chol are based on DSC[4] and fluorescence spectroscopic data, and are considered tentative.

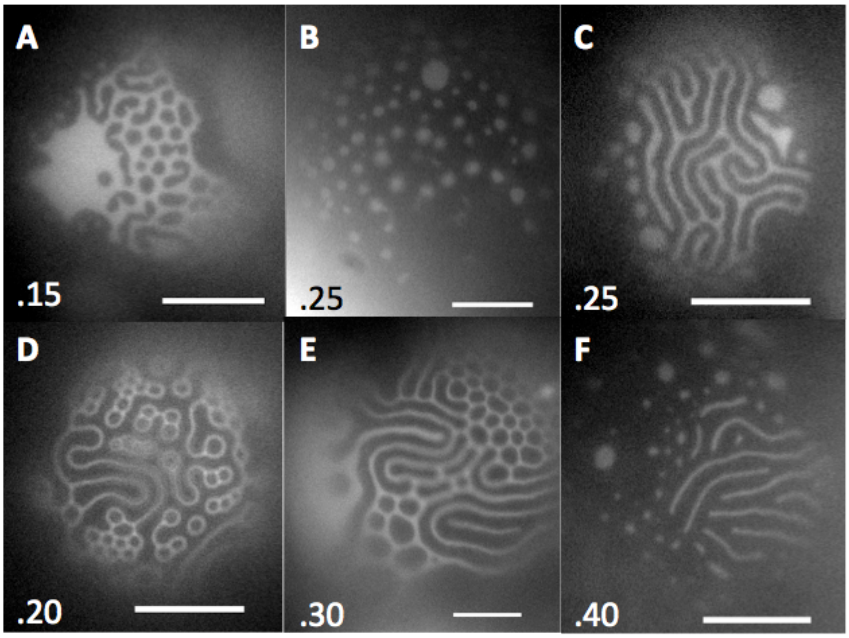

Figure S2 Fluorescence micrographs of GUVs show modulated phase patterns in the non-hybrid lipid mixture DSPC/(DLPC+DOPC)/Chol. When liquid phases coexist, the fluorescent dye C12:0-DiI partitions strongly into the Ld phase (bright regions) and is excluded from Lo phase. Images were taken at sample compositions A (upper panel, *A*-*C*) and B (lower panel, *D*-*F*) as listed in Table S1. Corresponding ρ values are indicated in the lower left corner of each image. Temperature 23 ºC; scale bar 10 μm.

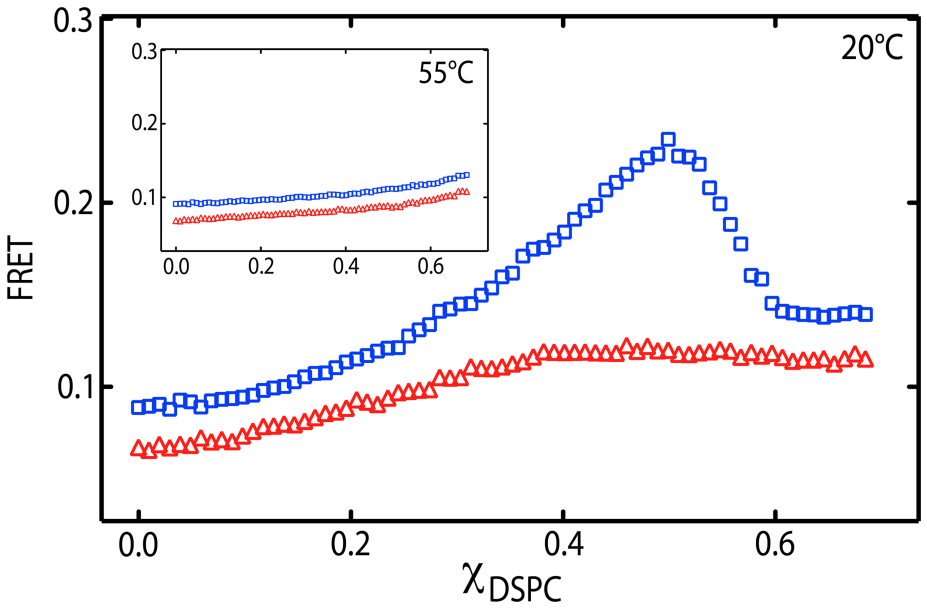

Figure S3 FRET reveals nanodomain formation in a non-hybrid lipid mixture. Sensitized acceptor emission is plotted *vs.* DSPC mole fraction for a sample trajectory composed of DSPC/(DLPC+DOPC)/Chol, at ρ = 0 (red triangles) and 0.25 (blue squares). Plots are offset by 0.02 y-units for clarity. Sample compositions are shown in Fig. S1 (orange line), and follow the approximate direction of tielines in the Ld+Lo region, passing through the SANS sample composition at DSPC/(DLPC+DOPC)/ Chol = 0.39/0.39/0.22. FRET efficiency is enhanced in phase coexistence regions where BoDIPY-PC donor and C12:0-DiI acceptor partition into the same (Ld) phase, behavior that is clearly observed in both sample trajectories at 20 ºC. *Inset*: the same samples measured at 55 ºC, revealing gradual changes consistent with uniform mixing.

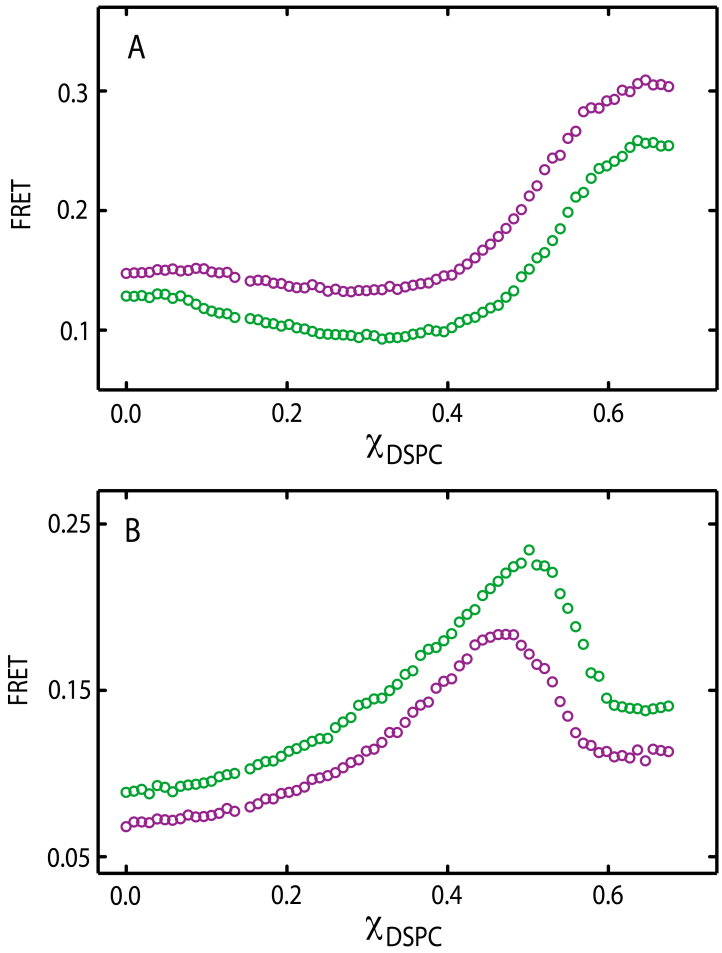

Figure S4 A comparison of FRET profiles between hybrid and non-hybrid lipid mixtures reveal similar trends in probe partitioning behavior. Sensitized acceptor emission is plotted *vs.* DSPC mole fraction for sample trajectories composed of DSPC/(POPC+DOPC)/Chol at 23 ºC for ρ = 0.20 (purple) and DSPC/(DLPC+DOPC)/Chol at 20 ºC for ρ = 0.25 (green). Plots are offset by 0.04 y-units (*A*) and 0.02 y-units (*B*) for clarity. Sample compositions follow the approximate direction of tielines in the Ld+Lo region of each mixture. (*A*) Regions of reduced FRET efficiencies are observed in both mixtures, where DHE donor and BoDIPY-PC acceptor partition into Lo and Ld phases, respectively. (*B*) Regions of enhanced FRET efficiencies are observed in both mixtures, where BoDIPY-PC donor and C12:0-DiI partition into the same (Ld) phase. Data for the DSPC/(POPC+DOPC)/Chol mixture taken from ref 17.

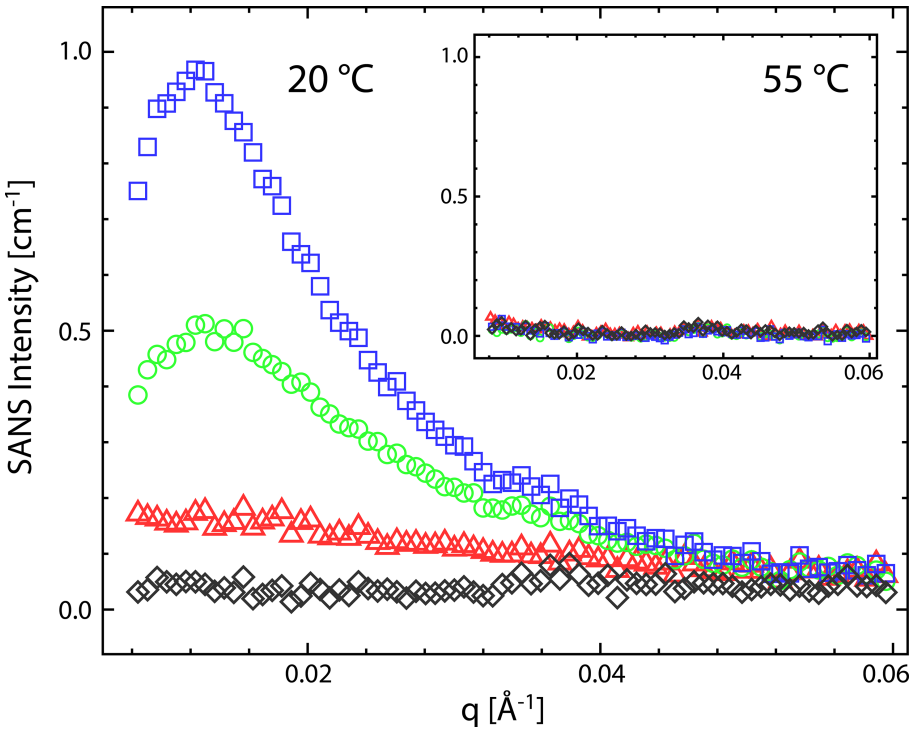

Figure S5 SANS reveals nanodomains in a non-hybrid lipid mixture. SANS intensity *vs.* momentum transfer vector q is shown for LUVs composed of DSPC/(DLPC+DOPC)/Chol = 0.39/0.39/0.22 at 20 ºC, for ρ = 0 (red triangles), 0.1 (green circles), and 0.25 (blue squares), and a single-phase control sample composed of DSPC/DLPC/Chol = 0.325/0.325/0.35 (black diamonds). *Inset*: the same samples measured at 55 ºC, revealing flat intensity consistent with uniform mixing. The small increase in scattering at $q < 0.02$ Å^{-1} seen in the 55 ºC data is likely the result of a small radial scattering length density contrast between the headgroup and acyl chain regions of the bilayer, while the small increase in scattering at $q \sim 0.035$ Å^{-1}, present in all curves, is an artifact from the data reduction software. Before fitting, these spurious contributions were corrected, as described in Section S1.3.

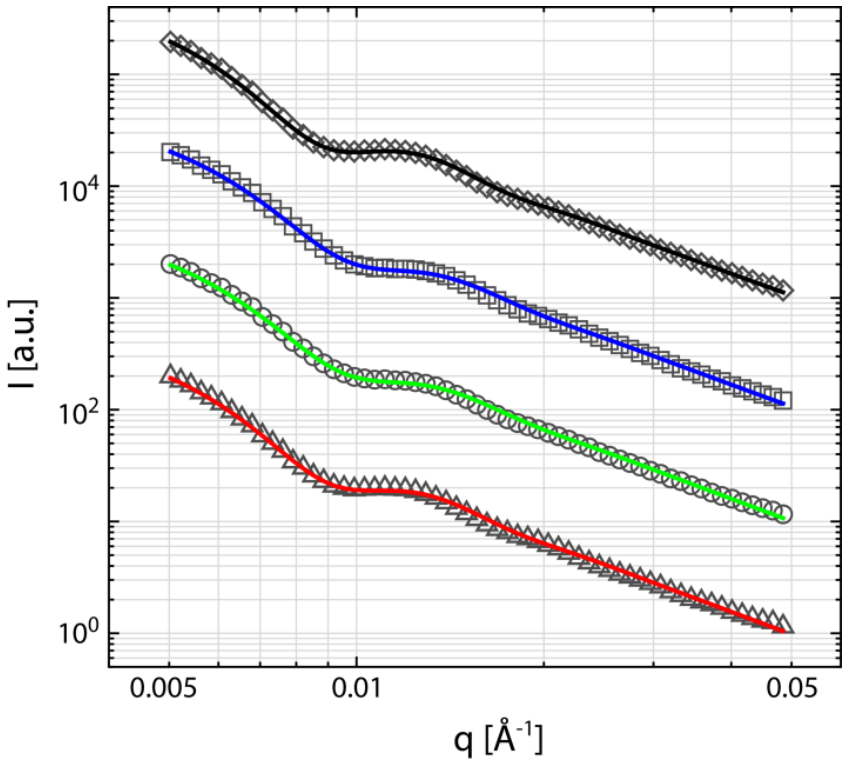

Figure S6 SANS data used to determine vesicle size and polydispersity. Shown are experimental SANS intensity *I* vs. momentum transfer vector *q* (symbols) and fits to the data (solid lines) for vesicles composed of: DSPC/(DLPC+DOPC)/Chol = 0.39/0.39/0.22 at 20 ºC, for ρ = 0 (triangles, red line), 0.1 (circles, green line), and 0.25 (squares, blue line); and DSPC/DLPC/Chol = 0.325/0.325/0.35 (diamonds, black line). Log-log curves are offset by powers of ten for clarity. Vesicle size and polydispersity were determined as described in Section S1.3; best-fit values are listed in Table S3.

S1. MATERIALS and METHODS

DSPC, DSPC-d70, DOPC, and DLPC were purchased as lyophilized powders or chloroform stocks from Avanti Polar Lipids (Alabaster, AL). Cholesterol was purchased from Nu Chek Prep (Elysian, MN). Stock solutions were prepared by dissolving lipid or cholesterol in HPLC-grade chloroform. Phospholipid purity of ≥ 99% was confirmed by TLC on washed, activated Adsorbosil TLC plates (Alltech, Deerfield, IL), developed with chloroform/methanol/water in a 65/25/4 ratio. Concentration of phospholipid stocks was determined to within 1% by inorganic phosphate assay.[5] Ultrapure H_2O was obtained from a Barnstead purification system (Dubuque, IA), and 99.8% D_2O was purchased from Alfa Aesar (Ward Hill, MA).

S1.1 Fluorescence microscopy

S1.1.1 Preparation of GUVs. GUVs were prepared using a modified version of the electroformation method.[6] Lipid films were swelled at 55 ºC in 100 mM sucrose in an AC field of 5 Hz (1 Vpp) for 2 h to form GUVs, then cooled to room temperature (23 ºC) over 12 h. The GUVs were then diluted into 100 mM glucose before imaging. The difference in solution density allows vesicles to settle more efficiently and also creates a sufficient refractive index difference to enable locating and focusing on GUVs without intense illumination.[7]

S1.1.2 Image data collection. Wide-field microscopy was performed on a Nikon Diaphot-TMD (Micro Video Instruments Inc., Avon, MA and Rochester, NY) at 23 °C using a 60× 1.4 numerical aperture oil immersion objective. GUVs were labeled with C12:0-DiI at 0.02 mol%; the dye partitions preferentially into the Ld phase. To minimize light-induced artifacts, GUVs were located with transmitted light prior to exposure to the intense illumination needed for fluorescence imaging. Images were taken with a Photometrics (Tucson, Arizona) CoolSNAP HQ2 charge-coupled device camera. C12:0-DiI was imaged with 530-550 nm excitation and 565-610 nm emission. Images were contrast-enhanced and analyzed with NIS Elements Basic Research Software (MVI, Inc.).

S1.2 Förster resonance energy transfer (FRET)

S1.2.1 Preparation of PLVs. FRET samples were prepared as previously described,[8] with the following modifications. Two series of samples (trajectories) were prepared at $\rho = 0$ and $\rho = 0.25$, each at ~ 1% compositional resolution along a presumed tieline within the Ld+Lo region of DSPC/(DLPC+DOPC)/Chol. Endpoint compositions of this tieline trajectory were (DLPC+DOPC)/Chol = 0.905/0.095 and DSPC/Chol = 0.685/0.315. FRET samples received fluorescent dyes in the following dye:lipid ratios: DHE, 1:100; BoDIPY-PC, 1:1500; and C12:0-DiI, 1:2000. Single-dye controls with the same dye:lipid ratios were prepared at ~ 10%

compositional resolution along the trajectory. For samples or controls containing 1% DHE (a cholesterol analog), cholesterol concentrations were reduced by 1%.

Paucilamellar vesicles (PLVs) in aqueous suspension were formed using the rapid solvent exchange (RSE) method,[9] in order to avoid a dried lipid film state that may accelerate the precipitation of cholesterol crystals. Briefly, 0.500 mL of aqueous RSE buffer (5 mM PIPES, 200 mM KCl, 1 mM EDTA, pH 7.0) was added to lipid mixtures dissolved in < 0.1 mL chloroform. The sample was then subjected to vacuum for ~ 1 min while vortexing to remove the chloroform, resulting in the formation of fully hydrated bilayers containing one to a few lamellae. Samples were then ramped from 50 to 20 °C at 2 °C/h in a water bath, and held at 20 °C for at least 36 h before data collection.

S1.2.2 FRET data collection. Fluorescence data were collected on a F7000 spectrofluorimeter (Hitachi High Technologies America, Schaumburg, IL) equipped with a temperature-controlled cuvette holder (Quantum Northwest, Inc., Liberty Lake, WA). Prior to measurement, samples were diluted to 25 μM total phospholipid in the cuvette with RSE buffer, while applying gentle stirring. Fluorescence intensity was measured in 6 excitation/emission channels (λ, nm), using 5 nm bandpass for excitation and emission slits, and 2 s integration time: DHE fluorescence (327/393); BoDIPY-PC sensitized emission (327/517); BoDIPY-PC fluorescence (505/517); C12:0-DiI sensitized emission (505/565); C12:0-DiI fluorescence (549/565); and vesicle scattering (430/420).

S1.2.3 FRET data analysis. The characteristic profiles of steady-state probe-partitioning FRET (SP-FRET) have been used to determine phase coexistence regions for samples prepared along a trajectory in composition space.[8,10] Abrupt changes in the lateral distribution of mixture components occurs at phase boundaries, resulting in changes in the energy transfer efficiency between fluorescent donor and acceptor lipids. For donor and acceptor that partition favorably into the same phase, a hill-shaped region of enhanced FRET efficiency (REE) is observed for samples located between phase boundaries, while a valley-shaped region of reduced FRET efficiency (RRE) is observed when donor and acceptor prefer different phases. We utilized two sensitized acceptor emission (SAE) channels for comparing SP-FRET along tieline trajectories. SAE channels contain non-FRET contributions from vesicle scattering, as well as direct donor and acceptor fluorescence emission; these spurious contributions were corrected using control samples.[8] Furthermore, an internal normalization that corrects for some sample-to-sample variation (*e.g.*, small concentration errors due to liquid transfers and differences in applied vacuum) was applied:

$$FRET = \frac{F_{SAE}}{\sqrt{F_D \cdot F_A}}$$

where F_{SAE}, F_D and F_A are scattering-corrected intensities from the SAE, donor and acceptor channels, respectively. The corrected FRET signal is plotted in Figs. 3 and S3.

To determine the location of the Ld+Lo phase boundaries, we used the SP-FRET profile of DHE donor and BoDIPY-PC acceptor, which displayed an RRE (Fig. 3). The phase boundaries at the left and right end of the trajectory were determined using the segmental linear regression function in Prism (v5.0d, GraphPad Software Inc., San Diego, CA). The intersection point of two straight-line regions in the vicinity of a phase boundary was determined for the data collected at 20 °C (see Fig. 3).

S1.3 Small-angle neutron scattering (SANS)

S1.3.1 Preparation of LUVs. Large unilamellar vesicles (LUVs) were prepared by extrusion as follows. Lipid mixtures were prepared by transferring desired volumes of chloroform stock solutions to a glass culture tube with a syringe (Hamilton USA, Reno, NV). Chloroform was removed with an N_2 stream and gentle heating, followed by drying *in vacuo* for a minimum of 12 h. Dry lipid films were hydrated with an appropriate D_2O/H_2O mixture (see below) preheated to 50 °C, followed by vigorous vortexing to disperse the lipid. The resulting multilamellar vesicle (MLV) suspension was incubated at 50 °C for 1 hour, and then subjected to 5 freeze/thaw cycles between –80 and 50 °C to reduce the average number of lamellae and facilitate extrusion. LUVs were prepared with a hand-held miniextruder (Avanti Polar Lipids, Alabaster, AL), assembled with a 50 nm pore-diameter polycarbonate filter and heated to 50 °C. The suspension was passed through the filter a minimum of 31 times, in all cases using an odd number of passes to minimize contamination with unextruded starting material. Data was collected within 24 h of extrusion. Final sample concentrations were 10-15 mg/mL, which allows for sufficient water between vesicles to eliminate the interparticle structure factor, thereby simplifying data analysis.

We performed two different types of SANS experiments, designed to isolate either the lateral bilayer structure (for examining domain formation), or the transverse bilayer structure (for vesicle size determination). Interrogation of lateral structure requires the use of a chain-perdeuterated species to provide neutron scattering length density (SLD) contrast upon demixing of lipids. Here, the high-melting lipid component was composed of DSPC and DSPC-d70 in a 42/58 ratio, yielding an average SLD for the bilayer's acyl chain region that is simultaneously equal to (1) the SLD of the bilayer's headgroup region, and (2) the SLD of water composed of 34.6 volume percent D_2O. This simultaneous contrast matching minimizes scattering associated with transverse structure, and enhances scattering due to demixing of saturated and unsaturated lipids (*i.e.*, domain formation). To determine the vesicle size distribution for each sample, a 0.200 mL aliquot was diluted with 0.400 mL of D_2O for a final D_2O concentration of 78 volume percent, thereby providing a large SLD contrast between the water and bilayer, and enhancing the spherical vesicle form factor.

S1.3.2 SANS data collection. Neutron scattering experiments were performed at the CG-3 Bio-SANS instrument of the High Flux Isotope Reactor (HFIR), located at Oak Ridge National Laboratory (ORNL). LUV suspensions were loaded into 1 mm path-length quartz banjo cells (Hellma USA, Plainview, NY) and mounted in a temperature-controlled cell holder with ~ 1 °C accuracy. Sample-to-detector distances of 2.5 and 15.3 m, and 6 Å wavelength neutrons (FWHM 15%) were used to obtain the relevant momentum transfer vector, $q = 4\pi \sin(\theta)/\lambda$, where λ is the neutron wavelength and 2θ is the scattering angle relative to the incident beam. Scattered neutrons were collected with a two-dimensional (1 m × 1 m) ^{3}He position-sensitive detector with 192 × 256 pixels. The 2D data were reduced following standard procedures using MantidPlot (http://www.mantidproject.org/). During reduction, the measured scattering intensity was corrected for detector pixel sensitivity, dark current, sample transmission, and background scattering contributions from the water and empty cell. The one-dimensional scattering intensity $I(q)$ was obtained by radial averaging of the corrected 2D data.

S1.3.3 SANS data analysis. The average vesicle radius and polydispersity were determined using the method of separated form factors described previously.[11] Briefly, data from high-contrast LUVs (*i.e.*, LUVs in 78 volume percent D_2O, Fig. S6) were fit to a spherical shell form factor with a Schulz size distribution, using a standard three-shell model (headgroup/hydrocarbon/ headgroup) to represent the flat bilayer form factor.

Domain sizes were determined by fitting data from radially contrast-matched samples (*i.e.*, LUVs in 34.6 volume percent D_2O, Fig. S5). Prior to analysis, SANS curves were corrected for small, spurious scattering contributions seen most clearly in the 55 ºC data (Fig. S5). A small increase in scattering at $q < 0.02$ Å^{-1} is likely the result of a residual radial SLD contrast between the headgroup and acyl chain regions of the bilayer (*i.e.*, incomplete contrast matching), while the small increase in scattering at $q \sim 0.035$ Å^{-1}, present in all curves, is an artifact from the data reduction software. These temperature-independent contributions were eliminated by subtracting the 55 ºC data from the corresponding 20 ºC data. We also fit the uncorrected data and found no significant differences in the obtained domain sizes, compared to the corrected data.

Corrected SANS data were modeled with a Monte Carlo method previously described in detail.[12] Briefly, vesicles were approximated as spherical shells of radius R and thickness t corresponding to the hydrophobic thickness of the bilayer, with polydispersity assumed to follow a Schulz distribution.[11] The shell volume was further divided into N monodisperse, randomly placed, non-overlapping caps (domains), each subtending an angle 2α. For the compositions studied, these domains are considered to be Ld phase dispersed in a continuous Lo matrix; the composition and total area fraction of the domains were calculated from phase boundaries determined by FRET data (Section S1.2) and published lipid volumes.[13] With the size and location of domains specified, random points were generated within the shell volume in proportion to the SLD

contrasts of the phases using a rejection algorithm (*i.e.*, points were uniformly generated within the shell and tested for inclusion in a domain until both the Ld and Lo volumes accumulated the desired number of points). The SLD-contrast-weighted pair distance distribution *P(r)* for the vesicle was then calculated from the set of random points following Henderson,[14] and the procedure was repeated for 10^5 vesicles to obtain an ensemble average. The scattering intensity is the Fourier transform of the averaged *P(r)*:

$$I(q) = \frac{1}{4\pi}\int P(r)\frac{\sin(qr)}{qr}dr$$

I(q) was smeared with the instrumental resolution function[15] and compared to experimental data using a standard χ^2 goodness-of-fit criterion, varying *N* until a best fit was achieved. The reported domain size is that corresponding to a Schulz distribution of vesicles, each containing *N* monodisperse domains, and therefore represents an average domain size consistent with the experimental data.

References

(1) Zhao, J.; Wu, J.; Heberle, F. A.; Mills, T. T.; Klawitter, P.; Huang, G.; Costanza, G.; Feigenson, G. W. *Biochim. Biophys. Acta* **2007**, *1768*, 2764.

(2) Feigenson, G. W. *Annu. Rev. Biophys. Biomol. Struct.* **2007**, *36*, 63.

(3) Zhao, J.; Wu, J.; Shao, H.; Kong, F.; Jain, N.; Hunt, G.; Feigenson, G. *Biochim. Biophys. Acta* **2007**, *1768*, 2777.

(4) Mabrey, S.; Sturtevant, J.M. *Proc. Natl. Acad. Sci. U.S.A.* **1976**, *73*, 3862.

(5) Kingsley, P.B.; Feigenson, G.W. *Chem. Phys. Lipids* **1979**, *24*, 135.

(6) Angelova, M. I.; Dimitrov, D. S. *Farad. Discuss.* **1986**, *81*, 303.

(7) Morales-Penningston, N. F.; Wu, J.; Farkas, E. R.; Goh, S. L.; Konyakhina, T. M.; Zheng, J. Y.; Webb, W. W.; Feigenson, G. W. *Biochim. Biophys. Acta* **2010**, *1798*, 1324.

(8) Heberle, F. A.; Wu, J.; Goh, S. L.; Petruzielo, R. S.; Feigenson, G. W. *Biophys. J.* **2010**, *99*, 3309.

(9) Buboltz, J. T.; Feigenson, G. W. *Biochim. Biophys. Acta* **1999**, *1417*, 232.

(10) Buboltz, J. T. *Phys. Rev. E* **2007**, *76*, 021903.

(11) Pencer, J.; Krueger, S.; Adams, C. P.; Katsaras, J. *J. Appl. Crystallogr.* **2006**, *39*, 293.

(12) Heberle, F. A.; Petruzielo, R. S.; Pan, J.; Drazba, P.; Kučerka, N.; Standaert, R. F.; Feigenson, G. W.; Katsaras, J. *J. Am. Chem. Soc.* **2013**, *135*, 6853.

(13) Kučerka, N.; Nieh, M.-P.; Katsaras, J. *Biochim. Biophys. Acta* **2011**, *1808*, 2761.

(14) Henderson, S. J. *Biophys. J.* **1996**, *70*, 1618.

(15) Qian, S.; Heller, W.T. *J. Phys. Chem B* **2011**, *115*, 9831.

(16) Goh, S.L.; Amazon, J.J.; Feigenson, G.W. *Biophys. J.* **2013**, 104, 853.

(17) Goh, S.L. *Cornell University*. **2013**. (Doctoral Dissertation, Accession Order No. 3571246).